ChemElectroChem

Research Article
doi.org/10.1002/celc.202400168

Chemistry Europe
European Chemical Societies Publishing

www.chemelectrochem.org

Lutetium Copper@Hexagonal Boron Nitride Nanocomposite Electrode System for Sensing and Signalling Ciprofloxacin

Collen Nepfumbada,[a] Bhekie B. Mamba,[a] Bart M. Bartlett,[a, b] Jorge F. Fernández-Sánchez,[c] and Usisipho Feleni*[a]

Herein, a new electrochemical sensing system based on lutetium copper nanoparticles supported on hexagonal boron nitride (Lu-Cu@h-BN) was designed for the sensitive detection of ciprofloxacin (CIP) antibiotic. A simple hydrothermal method was used to synthesize the nanocomposite. The structural and morphological characteristics of the as-prepared nanocomposite were investigated using various analytical techniques such as Fourier transform infrared spectroscopy (FTIR), X-ray diffraction (XRD), scanning electron microscopy (SEM), and X-ray photoelectron spectroscopy (XPS). The newly developed Lu-Cu@h-BN nanocomposite was used as an electrode modifier for sensing and signalling of CIP. Cyclic voltammetry (CV) and electrochemical impedance spectroscopy (EIS) were used to study the electrochemical activities of the bare GCE, Cu-h-BN/GCE, Lu-h-BN/GCE, Lu-Cu/GCE, and Lu-Cu@h-BN/GCE. The electro-oxidation of CIP on electrode surface exhibited an irreversible, diffusion-controlled process. The sensor system obtained a wider linear range of (0.05–100 μM) with a lower detection limit value of 0.03 μM and sensitivity 0.7443 $\mu A\,\mu M^{-1}\,cm^{-2}$. Furthermore, the sensor demonstrated an excellent selectivity, good stability, and reproducibility, with acceptable recoveries of 96% to 104% in real water sample analysis.

1. Introduction

Antibiotics are natural or synthesized antimicrobial compounds which are widely used in human and veterinary medicine to treat various infectious diseases.[1] However, antibiotics abuse may lead to pharmaceutical waste production which foul aquatic system, causing severe environmental problems like restriction of algae growth and stimulation of microbial resistance.[2] Ciprofloxacin (CIP) is a class of the newly developed fluoroquinolone (FQs) antibiotics employed against a broad-spectrum gram-negative and gram-positive infections.[3] CIP is used to cure variety of infectious diseases such as urinary tract infections, gastrointestinal infections, lower respiratory tract infections, pneumonia, skin and soft tissue infections due to the low cross-resistance.[4] Nevertheless, overuse of CIP drug can result in antibiotic resistance and ultimate treatment failure.[5] Therefore, it is crucial to monitor the presence and concentration of CIP into the environment.

Various analytical techniques have been reported for CIP detection, which include high-performance liquid chromatography (HPLC),[6,7] capillary electrophoresis (CE),[8] chemiluminescence,[9] and spectrophotometry.[10] Albeit their excellent sensitivity and reliability, they suffer from low selectivity, maintenance cost, and operational procedures. Therefore, to overcome the shortcomings of these traditional approach, research on the development of a rapid, reliable, selective, and efficient method for early detection of CIP is urgent and significant for environmental monitoring. Electrochemical methods offers a significant benefits over the previous reported techniques due to their admirable qualities, including high sensitivity, and selectivity, wide linear range, cost-effectiveness, low sample usage, portability and ease of operation.[11] CIP is regarded as an electroactive molecule that may be evaluated electrochemically due to its piperazine ring that oxidizes. Consequently, the electrochemical determination of CIP at the surface of electrodes has been reported by a number of researchers.[12] Different working electrode (WEs) such as screen-printed electrodes (SPEs), gold electrodes (AuE), glassy carbon electrodes (GCEs) among others have been reported for electrochemical sensing platform. Due to their affordability, usability, large specific surface area, and the possibility of miniaturization, GCEs are frequently used as WEs in electrochemical research. Despite these advantages, the low electron transfer rate at the interface and the target analyte causes the bare GCEs response to be poor. Modification of WEs with nanomaterials and nanostructures to attain high sensitivity, selectivity, conductivity, and fast electron transfer kinetics is an appropriate solution

[a] C. Nepfumbada, Prof. B. B. Mamba, Prof. B. M. Bartlett, Prof. U. Feleni
Institute for nanotechnology and water sustainability (iNanoWS)), College of Science, Engineering and Technology (CSET), University of South Africa (UNISA), Florida campus, 1709 Johannesburg, South Africa
E-mail: feleni@unisa.ac.za

[b] Prof. B. M. Bartlett
Department of Chemistry, University of Michigan, Ann Arbor, Michigan 48109-1055, United States

[c] Prof. J. F. Fernández-Sánchez
Department of Analytical Chemistry, University of Granada, 18071 Granada, Spain

to address this issue.[13,14] For instance, a GCE modified with CNOs/PANI-NTs/AuNPs nanocomposite was proposed by[15] as a nanostructured platform for the determination of CIP with a detection limit of 5 nM to 80 μM. In another study, a PEI@Fe_3O_4@CNTs modified GCE was fabricated for the determination of CIP with detection limit of 3.0 nmol L^{-1}.[16] The excellent performance of modified electrodes depends upon nature of the modifiers. Over the past few years, 2D carbon materials such as graphene (GR),[17] graphene oxide (GO),[18] multi-walled carbon nanotube,[19] reduced graphene oxide (rGO),[20] has been widely explored in the electrochemical field. However, the loss of effective surface area is the inevitable consequence of the aggregation or restacking of graphene sheets caused by the strong π interactions. Compact graphene film development on electrode surfaces decreases the electrode's surface area and slows down electrolyte transport, which lowers the electrode performance.[21] Among the 2D nanomaterials, hexagonal boron nitride (h-BN) has attracted considerable attention due to its properties such as high resistive nature towards oxidation, low cytotoxicity, high thermal and chemical stability, easy dispersion in water, and good mechanical strength, giving rise to a variety of potential applications.[22] Furthermore, owing to the presence of point defects in the crystal structure, the direct electron transfer is processed and hence offers good electrochemical activity.[23,24] According to recent literature, the use of h-BN significantly improves the electrochemical performance of a sensing device.[25] Previously, hBN composites such as AuNPs/POM/2D-hBN/GCE,[26] MIP/Fe@AuNPs/2D-hBN/GCE,[27] h-BN/HNTs/GCE,[28] FeVNPs/30hBN/SPCE,[29] 2D-hBN/f-MWCNTs (5 : 1)/GCE[30] were successfully employed for an electrochemical sensors fabrication.

This work aims to develop a sensitive, cost-effective, and selective electrochemical sensor based on lutetium copper nanoparticles supported on hexagonal boron nitride as electrocatalyst that will be responsible for the electro-oxidation of CIP antibiotic as a representative member of fluoroquinolones in water. The parameters for optimal performance of the prepared Lu-Cu@h-BN/GCE sensor were assessed to obtain precise evaluations of its performance concerning sensitivity and selectivity in buffered solution and wastewater sample. More importantly, the analytical performance of the proposed sensor at low analyte concentrations was investigated using square wave voltammetry to ascertain its importance in detecting trace concentration of CIP which is normally present in water body. To the best our knowledge, this is the first report on Lu-Cu@h-BN that explores the electrochemical sensing of CIP. The developed electrochemical sensor displayed extremely high catalytic activity, wide linear range, a low detection limit, good selectivity, stability, and reproducibility. We believe this study will provide new insight into the exploration of h-BN combined with metals nanoparticles in electrochemical sensing applications.

Experimental Section

Materials and Reagents

Sodium hydroxide (NaOH), disodium hydrogen phosphate (Na_2HPO_4), sodium dihydrogen phosphate (NaH_2PO_4), ethanol (C_2H_5OH), tert-butanol ($(CH_3)3COH$), boron nitride powder (BN~1 μm, 98 %) lutetium nitrate $Lu(NO_3)_2$, copper nitrate $Cu(NO_3)_2$, hexacyanoferrate(III) ($[Fe(CN)_6]^{3-/4-}$) ion and ciprofloxacin ($C_{17}H_{18}FN_3O_3$) were purchased from Sigma Aldrich, Johannesburg, South Africa. Na_2HPO_4 and NaH_2PO_4 were used for the preparation of phosphate buffer solution (PBS). Deionize water was used during synthesis procedure and for the preparation of electrolyte solution. All the reagents were used without further purification.

Instrumentation

The morphology and elemental composition of the samples were examined using scanning electron microscopy equipped with energy dispersive X-ray (SEM-EDX) JSM-IT300 Joel, Tokyo, Japan with an acceleration voltage of 20 kV. The chemical composition was further studied using X-ray photoelectron spectroscopy (XPS, Physical Electronics, USA) equipped with monochromatic Al-Kα excitation source. Infrared spectral analysis was conducted to determine the chemical structure in KBr pellet mode technique using a Fourier transform infrared (FT-IR) spectroscopy (Perkin Elmer spectrum 100 FT-IR, Waltham, MA, USA). The X-ray diffraction (XRD) patterns were obtained with a Bruker D8 Advance diffractometer with Cu Ka1 radiation at room temperature. The electrochemical studies were performed using a Biologic potentiostatic mode technique (AUT 83909, Autolab, South Africa). The electrochemical features of modified electrodes were evaluated using cyclic voltammetry (CV), electrochemical impedance spectroscopy (EIS) and square wave voltammetry (SWV).

Synthesis of Lu-Cu@h-BN Nanocomposite

A hydrothermal method was used for the synthesis of Lu–Cu@h-BN in accordance to the previous report[31] with slight modification. 0.512 g $Lu(NO_3)_2 \bullet H_2O$ and 0.425 g $Cu(NO_3)_2 \bullet 3H_2O$ were dissolved in 25 mL deionized (DI) water. Then 20 mL tert-butanol solution of 0.0679 g h-BN was added and stirred for 1 h. The reaction solution was then transferred to an autoclave to react at 160 °C for 6 h. Afterwards, the product was centrifuged at 4000 rpm, washed with absolute ethanol and DI water multiple times to remove all the impurities. The obtained product was then dried in an oven at 70 °C for 2 h. Thus, the powder produced was denoted as Lu-Cu@h-BN nanocomposite.

Modification of GCE with Lu-Cu@h-BN Nanocomposite

Prior to surface modification, the GCE working electrode (WEs) was polished using 1.0 μm, 0.3 μm and 0.05 μm alumina slurry on polishing pads. Deionized (DI) water and ethanol was further used to wash the GCE under ultrasonication and then the electrode was allowed to dry at room temperature. Ultimately, the cleaned electrode was used as the WEs in the study. Approximately 1 mg of the prepared materials, Lu-CuNPs, Lu-h-BNNPs, Cu-h-BNNPs, and Lu-Cu@h-BN nanocomposite were dispersed in 1 mL of DI water and sonicated for 30 min and 8 μL of resultant solutions were separately drop casted onto the surface of the GCE overnight at room temperature. The schematic illustrations showing the preparation of Lu-Cu@h-BN nanocomposite and Lu-Cu@h-BN/GCE sensor is presented in Figure S1 A & B.

2. Results and Discussion

2.1. Characterization Material

Figure 1 shows the top-view SEM image of the as-prepared Lu-Cu@h-BN nanocomposite, which reveals a spherical particles structure with no apparent agglomeration. From the highly magnified SEM image, inset in Figure 1A, it can be observed that the particles showcase a flakes-like sheets morphology with particle size ranging from 18–27 μm, as depicted in the normal distribution plot Figure 1B. Furthermore, EDS spectrum as an inset in Figure 1A, reveals the presence of lutetium (Lu), copper (Cu), boron (B), oxygen and nitrogen (N). Thus, presence of these elements confirms the formation of Lu-Cu@h-BN nanocomposite.

The crystallinity of the prepared materials was evaluated using powder XRD analysis. The XRD patterns of the as-prepared materials Lu-BNNPs, Cu-BNNPs, Lu-CuNPs, and Lu-Cu@h-BN nanocomposites are presented in Figure 1C. The XRD patterns were recorded in the 2θ ranging from 20° to 80° at room temperature. The XRD patterns of Lu-BNNPs and Cu-BNNPs displays a distinctive graphite-like peak at 26.6° 2θ correspond to (002) planes of h-BN, matching with (JCPDS card no. 34-0421).[32] It was notices that the diffraction peaks for h-BN was weak which suggest to its small size and low crystallinity. Figure S2 shows the XRD patterns of the bulk-h-BN. The diffraction patterns of the Lu-Cu nanoparticles matches the (JCPDS card no. 00-034-0394) for lutetium.[33] Furthermore, the diffraction pattern from the metallic copper (Cu) and copper oxide (CuO) were observed with (JCPDS card no. 45-0937) and (JCPDS card no. 04-0836), respectively [34][35]. The formation of CuO phase may be ascribed to the alkaline solution used during synthesis and the fact that oxygen has strong affinity towards metals to form stable metal oxide. A sharp and intensive diffraction peaks highlight its high crystallinity. Lastly, all the indexed peaks corresponding to Lu-BNNPs, Cu-BNNPs and Lu-CuNPs are present in Lu-Cu@h-BN indicating that the nanocomposite was successfully synthesized without any external impurities.

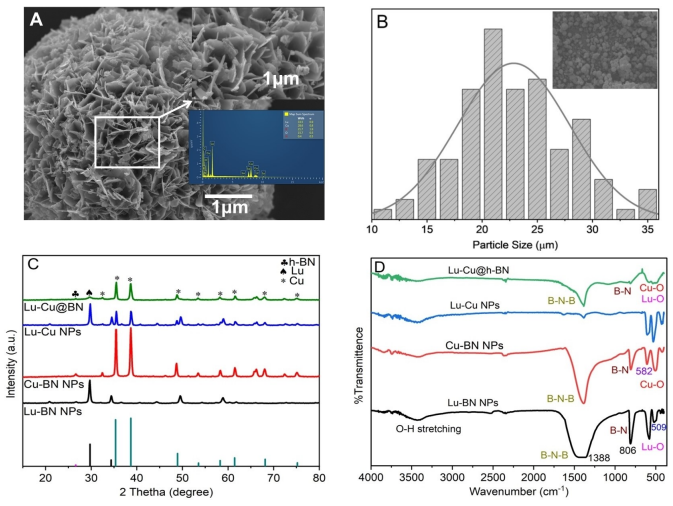

Figure 1. SEM-EDS and size distribution of Lu-Cu@h-BN (A–B) XRD patterns (C) FTIR spectra (D) of Lu-BNNPs, Lu-CuNPs, Cu-BNNPs and Lu-Cu@h-BN nanocomposite, respectively.

FTIR spectra of Lu-BNNPs, Lu-CuNPs, Cu-BNNPs, and Lu-Cu@h-BN nanocomposite were obtained to investigate the functional groups and it was recorded in the range from 400–4000 cm^{-1}. As shown in Figure 1D, two characteristic h-BN peaks at 1388 cm^{-1} and 806 cm^{-1} corresponding to the B–N in-plane transverse stretching mode (E_{1u}) and B–N–B out-of-plane bending mode (A_{2u}) was observed from the FTIR spectra of Lu-BNNPs and Cu-BNNPs, respectively. These two characteristic peaks agree with those of the bulk h-BN (Figure S3). The broad absorption peak between 3400 cm^{-1} and 3500 cm^{-1} can be ascribed to the OH stretching vibrations.[36] In addition, the FTIR shows a visible weak band obtained between 400 to 600 cm^{-1} which correspond to the metal oxide from Lu–O and Cu–O, respectively [37][38]. The FTIR spectrum of the as-prepared nanocomposite shows all the absorption peaks observed in Lu-BNNPs, Lu-CuNPs and Cu-BNNPs. However, it was worth noting that the characteristic vibrational peak of B–N on the composite materials at 806 cm^{-1} was weakened compared to the other prepared nanoparticle indicating the succession on nanocomposite formation. Furthermore, no additional functional groups were present on the prepared nanocomposite. Hence, the FT-IR spectroscopic confirm the successful synthesis of Lu-Cu@h-BN composite material.

The XPS analysis was used to investigate the composition, chemical purity, and valance states of Lu-Cu@h-BN nanocomposite. The typical XPS survey spectrum of the as-prepared nanocomposite was analysed between 0 to 1200 eV providing the binding energies of the respective elements which also describe the purity of the samples as showed in Figure 2A. The peaks at 8,13, 187,86, 188.96, 284,8, 395,48, 930,33 eV, corresponding to Lu4f, Lu4d, B1s, C1s, N1s, O1s, and Cu2p elements are clearly seen in the spectrum, respectively. The peaks of Cu 2p, and Lu 4d correspond to the species in different states on the surface scales. The binding energies were calibrated using the standard C1s spectrum showing a peak at around 284.6 eV. The O1s spectrum shows a peak at around 530.1 eV originated from oxygen in metal-oxide (M–O) bonds.[39] The high-resolution spectra of B1s and N1s are positioned at binding energies close to 188.7 and 397.5 eV, respectively, corresponding to B–N bonds (Figure 2B & C). It is impossible to eliminate carbon contamination in almost all the sample preparations hence the C1s spectrum was observed at the binding energy of 284.6 eV. The XPS spectrum of the Cu2p core level region for the Lu-Cu@h-BN shows various peaks corresponding to the existence of mixed oxidation states of copper ions with Cu and Cu^{2+} states (Figure 2D). Two major broad peaks between 929.6 to 934.5 eV and 948.4 to 954.8 eV revealed the existence of metallic copper (Cu) and Cu^{2+} state and can be attributed to the binding energy of $Cu2p_{3/2}$ and $Cu2p_{1/2}$, respectively. Their satellite feature at the high binding energy centred between 935.6 to 943.8 eV and 958.7 to 963.4 eV of the Cu $2p_{3/2}$ corresponding to the characteristic of Cu–O peaks were observed, confirming that the Cu oxidation state is mainly + 2.[40,41] The Lu-Cu@h-BN also shows the Lu 4d spectrum

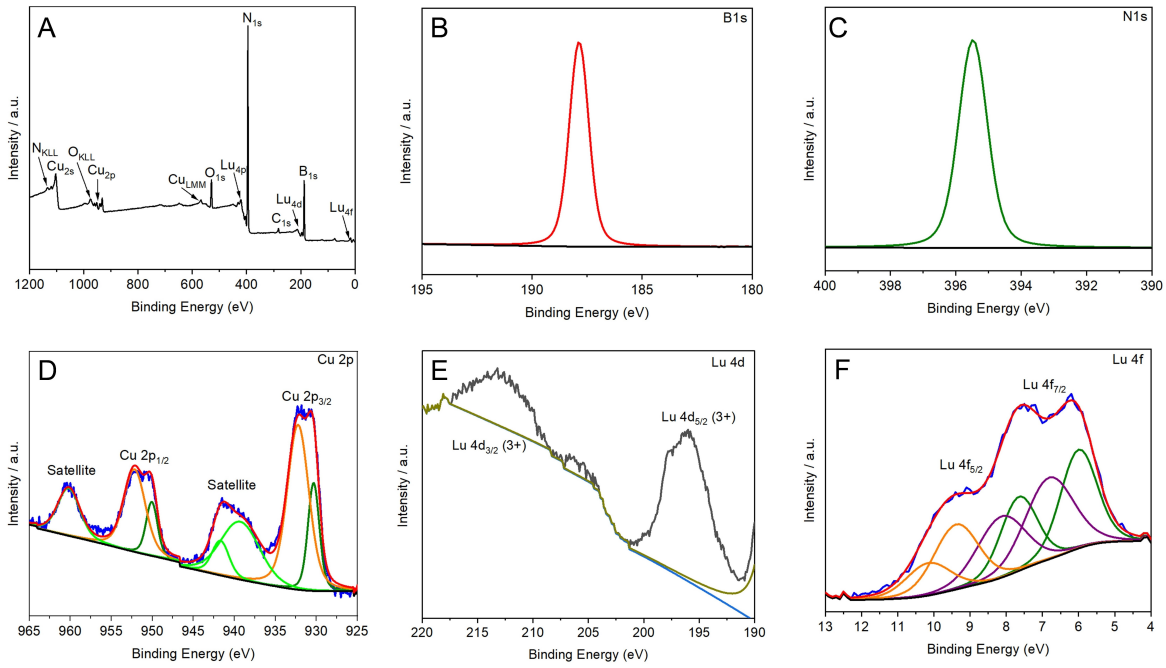

Figure 2. (A) XPS spectrum and deconvoluted curves of (B) B1s, (C) N1s, (D) Cu2p, (E) Lu4d and (F) Lu4f of the Lu-Cu@h-BN nanocomposite, respectively.

comprising of two peaks located at 196.7 eV and 213.1 eV, which corresponds to the Lu^{3+} oxide state (Figure 2E). Finally, from the Lu 4f spectrum (Figure F), peak between 5 and 12 eV values reveals that Lu exists in +3 oxidation state.[42] No foreign impurities were identified in the spectrum except that of carbon.

2.2. Electrochemical Characterization of Different Modified Electrode

The charge transfer ability is among the most important features in electrochemical devices and can be strongly influenced by the conductivity and the surface area of the working electrode, which can be easily assessed using cyclic voltammetry (CV) and electrochemical impedance spectroscopy (EIS) techniques.[12] Figure 3A shows the CV traces of bare GCE, Lu-Cu/GCE, Lu-h-BN/GCE, Cu-h-BN/GCE, and Lu-Cu@h-BN/GCE in standard redox system of 5 mM $[Fe(CN)_6]^{3-/4-}$ with supporting electrolyte of 0.1 M KCl solution at 50 mV s^{-1}. The two fundamental components that offers important information about the charge-transfer mechanism are the current of the oxidation and reduction peaks as well as the peak-to-peak separation (ΔE_p). It was observed that the bare GCE exhibited an oxidation reaction of $[Fe(CN)_6]^{3-/4-}$ with 0.1 M KCl at around 0.464 V with peak current response of 23.12 μA at a scanning rate of 25 mV s^{-1}. Additionally, the bare GCE had the highest peak $\triangle E_p$ of 0.510 V obtained from anodic peak potential at 0.464 V and cathodic peak potential at −0.046 V. When the GCE were modified with Lu-Cu/GCE, Lu-h-BN/GCE and Cu-h-BN/GCE, the peak currents were noticeably increased, while the ΔE_p values were decreasing from 0.207, 0.90 and 0.177 V, respectively. This result indicates that the nanoparticles can increase the electroactive surface area and conductivity, thus accelerating electron transfer between $[Fe(CN)_6]^{3-/4-}$ and the electrode surface.[43] However, when compared to the three modified electrode, the nanocomposite material (Lu-Cu@h-BN) exhibited higher peak current with lower $\triangle E_p$ (0.166 V), which could be due to the large specific surface area and strong conductivity enabling rapid electron transfer from the $[Fe(CN)_6]^{3-/4-}$ with 0.1 M KCl solution to the electrode surface achieving an

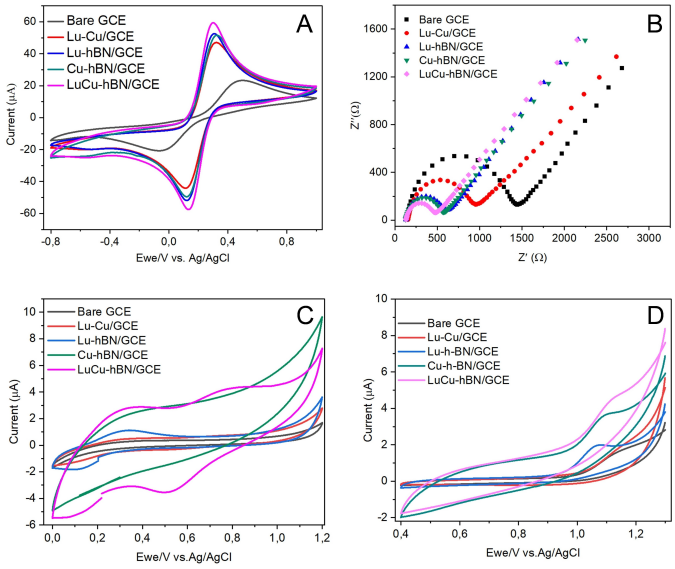

Figure 3. (A) CV curves of different modified electrodes. (B) EIS curves of different modified electrodes in 5 mM $[Fe(CN)_6]^{3-/4-}$ with 0.1 M KCl solution (C) in the absence of CIP (D) in the presence of 50 μM CIP in 0.1 M PBS electrolyte solution 50 mV s^{-1}.

oxidation peak current value of 59.36 μA. From the results, it can be concluded that the nanocomposite has high ability for electron transfer and can be regarded as good choice for sensing material.

EIS is another effective technique for examining the interfacial characteristics on the electrode surfaces. The conductivity of different electrodes can be obtained based on the charge transfer resistance (R_{ct}) value by selecting a suitable equivalent circuit model based on the reaction.[44,45] Figure 3B depicts Nyquist plots of bare GCE, Cu-h-BN/GCE, Lu-h-BN/GCE, Lu-Cu/GCE, and Lu-Cu@h-BN/GCE in 5 mM $[Fe(CN)_6]^{3-/4-}$ with 0.1 M KCl solution. It was observed that the diameter of the semicircle displayed by the bare GCE in the EIS was extremely wide which result to greater R_{ct} value, indicating poor conductivity of the electrode. After modifying the electrode with Cu-h-BN/GCE, Lu-h-BN/GCE and Lu-Cu/GCE, there was an apparent change in the diameter of the semicircle in the EIS corresponding to the charge transfer resistance, and it was observed to be smaller as compared to that of the bare GCE which indicate improvement of charge transfer on the working electrode surface. In addition, the modification of electrode with Lu-Cu@h-BN/GCE nanocomposite has notably lessened the diameter of the semicircle compared to the other modified electrodes, indicating small charge transfer resistance (R_{ct}) at the electrode–electrolyte interface and good conductivity.

For further investigations, CV was also used to assess the electrocatalytic properties of Cu-h-BN/GCE, Lu-h-BN/GCE, Lu-Cu/GCE, and Lu-Cu@h-BN/GCE in 0.1 M PBS (pH = 7.4) supporting electrolyte solution. Figure 3C shows the cyclic voltammograms recorded in the absence of CIP and reveals the redox peak brought about by the oxidation-reduction of copper and lutetium on Lu-Cu@h-BN/GCE modified electrodes.[46,47] The total current in CV comprises of two components, the non-faradaic capacitive current, which generates the background current, and the faradaic current, which is produced by faradaic reactions. Hence, in the absence of the analyte, only the background current was observed for Cu-h-BN/GCE, Lu-h-BN/GCE, Lu-Cu/GCE, and Lu-Cu@h-BN/GCE brought on by the capacitive current and comparable to that in the presence of 50μM CIP. This may be attributed to the increased in the electroactive surface area on the modified electrode which elevate the accumulation of the positively and negatively charged ions within the electrode surface. Consequently, the background current increases owing to an increase in capacitance and the double layer charging effect.[48,49] As expected, a larger background current recorded on Lu-Cu@h-BN/GCE compared to the other modified electrode was observed which is probably due the increase in electrode specific surface area which improves electrocatalytic activity.[50] Similarly, cyclic voltammetry was also used to study the electro-oxidation of CIP on Lu-Cu@h-BN/GCE in 0.1 M PBS (pH = 7.4) aqueous solution containing 50 μM CIP analyte. The CV responses obtained for the bare GCE, Cu-h-BN/GCE, Lu-h-BN/GCE, Lu-Cu/GCE, and Lu-Cu@h-BN/GCE modified electrodes at a scan rate of 50 mV s^{-1} are shown in the Figure 3D. The anodic peak centred at ~1.0 V relates to the irreversible electro-oxidation of CIP on modified electrodes which agrees to previous reports in literature.[51] The oxidation peak obtained for Lu-Cu/GCE is 4.2 μA which is significantly higher than that obtained for the bare GCE and other modified electrodes. The increase in peak current may be attributed to the improved in electroactive surface area and the number of active sites produced with incorporation of 2D-h-BN which facilitated electron transfer kinetics for the electrochemical oxidation of CIP.

2.3. Electrochemical Oxidation of CIP at Different pH and Scan Rate on Lu-Cu@h-BN

The pH of an electrolyte solution is an essential factor during detection, as it significantly influences the response of a sensing device as well as the reaction mechanism of the analyte on its surface. Generally, the signal varies across acidic, neutral, and alkaline conditions.[44] Herein, the effect of buffer pH on the oxidation response of Lu-Cu@h-BN/GCE toward 50 μM CIP was investigated by CV in 0.1 M PBS over the pH range (3, 5, 7 and 9) as illustrated in Figure 4A, B. It was clear that increasing pH from 3 to 9 leads to an initial rise and subsequent decline in oxidation peak current response, coupled with a leftward shift in peak potential, which indicates that the sensor performs better in more acidic electrolyte solution due to the involvement of protons during the oxidation of CIP.[2] Although the sensor exhibits maximum oxidation peak current response when pH = 3 compared to pH 5, a sharp peak with well define signature response of CIP was observed at pH 5 with current response not significantly lower to that of pH 3. Hence, pH 5 was chosen as optimal for subsequent experiment for electrochemical determination of CIP. Another important parameter that should be considered in the study of the effect of pH is the relationship between pH and peak potentials (E_{pa}) as depicted in Figure 4C. The results reveal the negative displacement of the peak potentials due to the increment of the pH of the electrolyte in a linear mode (E_{pa} (V) = −0.05322pH + 1.3072) (R^2 = 0.96811) proving the participation of protons in the redox process. Furthermore, the slope of this line is important in electroanalytical studies as it can be used to predict the number of electrons and protons involved in an electrochemical reaction Eq. (1).

$$\frac{\partial E_p}{\partial pH} = -2.303\ \frac{mRT}{nF} \quad (1)$$

where, m and n represent the number of protons and electrons and F (96.485 C mol^{-1}), T (298 K), and R (8.315 J mol^{-1} K^{-1}) refer to the Faraday constant, absolute temperature, and universal gas constant, respectively.[52] Since the slope of this line is close to the theoretical value of the Nernst equation (–0.0591 V pH^{-1}), it can be concluded that the number of electrons and protons in the oxidation reaction of CIP is equal. These results could be explained by the presence of zwitterion form of CIP in the acidic to basic conditions due to the deprotonation of –COOH group in one part and protonation of amino group in the piperazine ring. As a results, this suggests the possibility of electrostatic interaction between the active sites or the positively charged

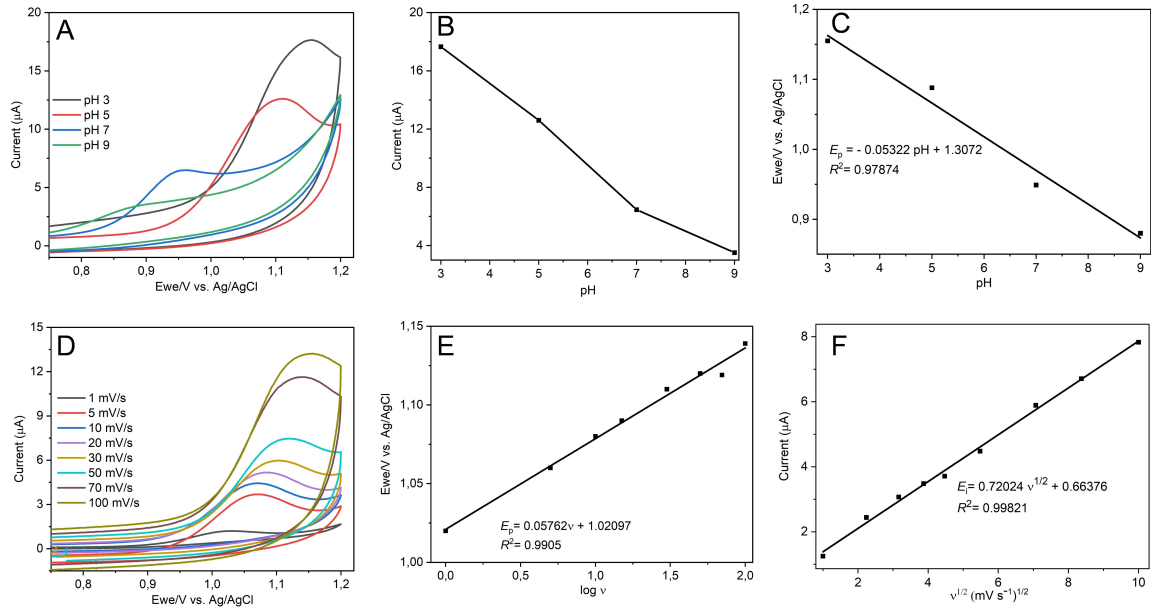

Figure 4. (A) CV responses of Lu-Cu@h-BN/GCE at different pH (b) Plot of peak current versus pH (C) linear plot of peak potential versus pH (D) CV responses at different scan rate (1–100 mV s^{-1}) of Lu-Cu@h-BN/GCE in 0.1 M PBS containing 50 μM ciprofloxacin (E) linear calibration plot between E_p and log of scan rate and (F) linear calibration plot between I_p and square root of scan rate.

metal sites in composite material with electron rich groups of CIP. Moreover, CIP can form stable complexes with metal cations via interaction between electron deficient metal ions in Lu-Cu@-h-BN (Cu^{2+}, Lu^{2+} and Lu^{3+}) and electron rich –COOH, amino group and heterocyclic group in CIP which facilitate the diffusion of CIP on the electrode surface and further oxidation of more CIP molecules on the Lu-Cu@h-BN/GCE.

To investigate the dynamic behaviour of CIP on the electrode surface, CV was used to establish the relationship between peak current and scanning rate. Figure 4D displays the CVs of 50 μM CIP at Lu-Cu@h-BN/GCE at different scan rates ranging from 1 to 100 mV s^{-1}. It was noticed that there is a progressive increase in oxidation peak current with increasing scan rates from 1 to 100 mVs^{-1} along with a shift in peak potential to a more positive value, confirming that the oxidation of CIP at the surface of Lu-Cu@h-BN/GCE is irreversible.[53] The plot of E_p versus log of scan rate (Figure 4E) is linear, with the regression equation $E_p = 0.0576 \log \nu + 1.021$ ($R^2 = 0.9905$). In addition, the plot of I_p (μA) versus square root of scan rate (Figure 4F) yields the regression equation I_p (μA) = $0.7018\ \nu^{1/2}$ (mVs^{-1}) + 0.8435, $R^2 = 0.9977$. The above results further confirm that the voltametric oxidation of CIP at the surface of Lu-Cu@h-BN/GCE is primarily an irreversible diffusion-controlled electrode process.[53] Moreover, the slope of Figure 4E can be used to calculate the electron transfer coefficient (α) using the Laviron's equation (RT/αnF = slope of E_p vs ln ν).[54] By assuming the number of electrons transferred (n) is 2, α is estimated to be 0.25 which is closer to the theoretical value (ranges from 0.3 to 0.7) for an irreversible electrode process. In short, from the kinetics study, it is confirmed that the oxidation of CIP on Lu-Cu@h-BN/GCE is a two-electron involved, diffusion controlled irreversible process. The proposed mechanism for electrocatalytic oxidation of CIP on Lu-Cu@h-BN/GCE is given in scheme 1 which is in accordance with the reported literatures.[55,56]

2.4. Effect of Different Concentrations

The electrocatalytic capability of the Lu-Cu@h-BN/GCE was explored using square wave voltammetry (SWV) with diverse CIP concentrations from 0.05 μM to 100 μM in 0.1 M PB electrolyte PBS (pH = 5.0) at a scan rate of 25 mVs^{-1}, as displayed in Figure 5A. It was notitced that, with an increase in CIP concentration, the I_{pc} of the Lu-Cu@h-BN/GCE increased linearly from 17 μA to 29.16 μA with a slight potential shift in E_{pc}, indicating the fast electron transfer kinetics. This result suggests that Lu-Cu@h-BN/GCE has excellent electrocatalytic features for the electro-oxidation of CIP. The sensor shows a linear current response in the concentration range 0.05 μM–100 μM. The gradual increase of anodic peak current displays two regression equation with correlation coefficient of $I_{pa} = 0.9527$ [CIP conc.] + 20.6093 ($R^2 = 0.923$) and $I_{pa} = 0.04027$ [CIP conc.] + 25.73948 ($R^2 = 0.967$) (Figure 5B), where [CIP conc.] denotes the concentration of CIP and I_{pa} denotes the peak current. This result could be explained by the fact that, low CIP concentration results in fast molecular movement leading to quick response whereas

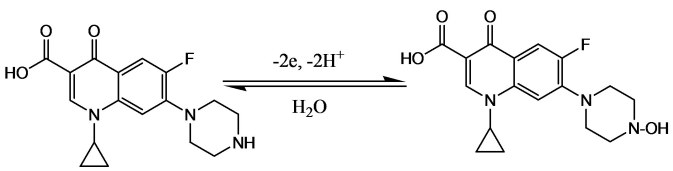

Scheme 1. Mechanism of electrochemical oxidation of ciprofloxacin.

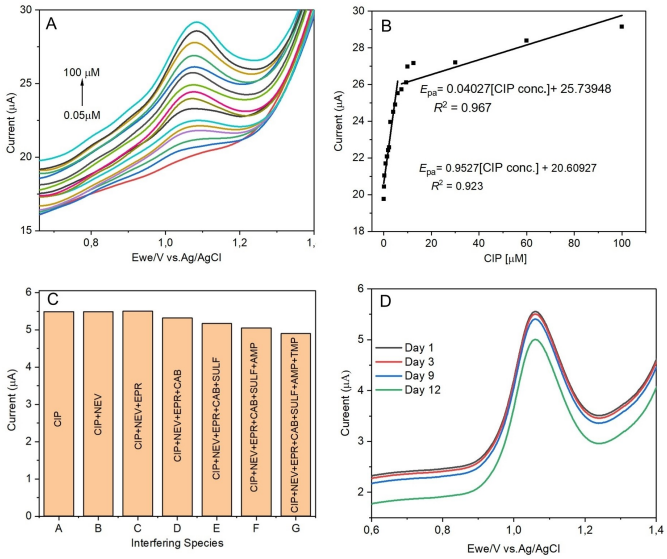

Figure 5. SWV responses of Lu-Cu@h-BN/GCE (A) variation in CIP concentration (0.05–100 μM) (B) linear plot of CIP concentration and log of peak current (C) interfering 10 μM CIP with 100 μM of NEV, EPR, CAB, SULF, AMP, and TMP (D) stability studies in a supporting electrolyte of 0.1 M PBS (pH = 5.0) at a scan rate of 25 mVs^{-1}.

Table 1. Comparison of analytical properties of different modified electrode for the determination of CIP.

Modified electrode	Method	Linear range (μM)	LOD (μM)	Ref.
MnO_2/ZnO/GCE	DPV	0.50–120	0.210	[57]
AuNP/CHI/SPE	SWV	0.10–150	0.001	[58]
V_2O_5/SPE	DPV	0.04–365	0.010	[59]
Ag_2MoO_4/GCE	CV	0.04–240	0.030	[60]
N-prGO/CPE	DPV	0.10–10	0.040	[61]
ChCl/CPE	SWV	0.005–200	0.004	[62]
GO/SPCE	DPV	1.0–8.0	0.300	[63]
CNOs/PANI-NTs/GCE	DPV	0.05–80.0	0.001	[15]
$ZnWO_4$/CB/GCE	DPV	0.0–100	0.020	[64]
Lu-Cu@h-BN/GCE	SWV	0.05–100	0.030	This work

higher concentration substantially obstruct the CIP movement. To determine the sensitivity, the regression equation in lower concentration range was considered. Thus, the sensitivity of the developed sensor is determined to be 0.7443 $\mu A\,\mu M^{-1}\,cm^{-2}$. Similarly, the electro-oxidation of CIP on Lu-Cu /GCE, Lu-h-BN/GCE, and Cu-h-BN/GCE were evaluated and their sensitivity were found to be 0.4771 $\mu A\,\mu M^{-1}\,cm^{-2}$, 0.3580 $\mu A\,\mu M^{-1}\,cm^{-2}$ and 0.3380 $\mu A\,\mu M^{-1}\,cm^{-2}$, respectively (Figure S4). The LOD of the modified electrode was calculated using the following Eq. (2)

$$LOD = \frac{3\sigma}{q} \quad (2)$$

where, σ is the standard deviation of the background and q is the slope obtained from the calibration curve at lower concentration. The calculated LOD of Lu-Cu/GCE, Lu-h-BN/GCE, Cu-h-BN/GCE and Lu-Cu@h-BN/GCE was found to be 0.54, 0.43, 0.38 and 0.03 μM, respectively. Therefore, it is evidence that the Lu-Cu@h-BN/GCE modified electrode has better response in comparison to the other modified electrode. Table 1 shows the comparisons between the Lu-Cu@h-BN/GCE sensor with other reported systems from the viewpoint of LOD and linear range. As can be seen, the Lu-Cu@h-BN based sensor was able to detect CIP even at low concentration and its LOD is comparable with those previously reported in literature.

2.5. Selectivity, Stability, and Reproducibility of Lu-Cu@h-BN/GCE

One of the primary objectives of the present study was to assess the ability of the proposed electrochemical sensor to quantify CIP in water sample. Thus, for an electrochemical measurement to be employed in practical settings, selectivity is a crucial parameter. A selective electrochemical sensor must have the ability to recognize the target analytes amid other potentially coexisting compounds. Therefore, to investigate the anti-interferents potency of Lu-Cu@h-BN/GCE, SWV responses was tested as shown in Figure 5C. The anti-interference ability was evaluated in the presence of 10 μM CIP with 100 μM of some potential and biological interferents, including Nevirapine (NEV), Eproxen (EPR), Carbamazepine (CAB), Sulfamethoxazole (SULF), Ampicillin (AMP), and Trimethoprim (TMP). It was noticed that, when CIP was mixed with CAB, there was an additional small peak at 0.8237 V, and SULF responded at the potential between 0.911 and 0.951 V (Figure S5). However, the voltametric oxidation signal of CIP was not significantly affected by the interferents, although the was a slightly shift in the peak potential after the addition of interfering molecules which could be due to the interaction occurring at the surface of the electrode. The relative error (%) was calculated and found to be around 5.14%. This result demonstrates that Lu-Cu@h-BN/GCE confirms good selectivity towards CIP with existing interferents compounds.

The performance of the proposed sensor was also monitored based on its stability and reproducibility. Thus, to test the stability of the sensor, Lu-Cu@h-BN/GCE was kept at ambient temperature over the period of 12 days and the measurements were taken every after 3 days. The voltametric response of the sensor was compared to the initial current of the modified electrode (Figure 5D). Initially, the sensor exhibited an oxidation peak current of 5.55 μA in the presence of 10 μM CIP. After 12 days, the current response decreased to 5.0 μA. The RSD calculated for the current responses was 10% indicating the supreme stability of the proposed Lu-Cu@h-BN/GCE sensor.

The reproducibility test was performed with four different Lu-Cu@h-BN/GCE modified electrodes. These electrodes were fabricated independently by the same procedure. This was evaluated by SWV responses for the oxidation of 10 μM CIP in

0.1 M PBS (pH 5.0) (Figure S6). The obtained RSD for the oxidation peak current responses was of 10%, suggesting that the proposed sensor has an excellent reproducibility for the electro-oxidation of CIP.

3. Real Sample

The practical applicability of the prepared Lu-Cu@h-BN/GCE sensor was estimated by the determination of CIP content in two wastewater samples colletced from Vulindlela and Mpangeni wastewater treatment plants in Kwazulu natal as well as the commercial pharmaceutical samples. Before analysis, the water sample was purified by filtering and pH was adjusted to the optimum value (pH 5). The standard addition technique was applied for CIP detection in all sample using the SWV technique. Initially, the background SWV scan was tested from the collected sample. Next a known concentations of CIP were spiked into the water sample, and the resuntant was analyzed using SWV (Figure S7A & B). Similarly, the commercial tablet dosage forms of CIP was used to understand the practical applicability of the newly developed Lu-Cu@h-BN/GCE sensor. After being ground into fine powders and dissolved in a 0.1 M PBS (pH 5) solution, the commercially available tablets were diluted to the desired working concentration and SWV was used to record the current responses (Figure S7C). As shown in Table 2, the recoveries of the detected samples ranged from 92% to 101%, with the RSD of less than 6%, indicating that the sensor could be successfully used to detect CIP in water sample.

4. Conclusions

In this report, the feasibility of attaining a portable, selective, and highly sensitive electrochemical sensor for detecting CIP antibiotics in wastewater was demonstrated by exploiting the synergistic effect on the electrode with conductive Lu-Cu@h-BN nanocomposite. Following optimization, Lu-Cu@h-BN/GCE sensor establishes appreciable affinity for CIP, with high sensitivity of 0.7443 $\mu A\,\mu M^{-1}\,cm^{-2}$, lower limits of detection, LOD = 0.03 μM and wide liner range 0.05 μM–100 μM. Interestingly, the sensor shows very strong selectivity for CIP, both in buffer and real wastewater samples as against closely and non-closely related antibiotics. Moreover, the sensor exhibits high stability and good reproducibility. Furthermore, the sensor displays good recoveries values, ranging from 92–104%, 96.0%–101% in WWT sample, and 98–125% in tablet, thereby validating its practical applicability in the intended media. Thus, the presented electrochemical platform displays potential capability as a portable and cost-effective sensor for CIP detection in wastewater. Further research is planned to extend the application of the developed sensor for selective detection of multiple Fluoroquinolones antibiotic targets.

Table 2. Detection of CIP in two real wastewater samples and tablet on Lu-Cu@h-BN.

Sample	Added (μM)	Found (μM)	Recovery (%)	RSD (%)
Vulindlela	1	0.92	92.0	6.0
	2	1.92	96.0	2.0
	3	3.04	101	1.0
Mpangeni	1	0.96	96.0	2.9
	2	2.09	104	3.1
	3	2.96	99.0	1.0
CIP tablet	1	1.25	125	5.2
	2	1.89	98	2.6
	3	3.25	108	3.5

Acknowledgements

The authors would like to thank the University of South Africa for the support in this project as well as the University of Michigan for XPS analysis.

Conflict of Interests

The authors declare that they have no known competing financial interests or personal relationships that could have appeared to influence the work reported in this paper.

Data Availability Statement

Data will be made available on request.

Keywords: Ciprofloxacin · detection · electrochemical sensor · hydrothermal method · nanocomposite

[1] M. Majdinasab, R. K. Mishra, X. Tang, J. L. Marty, *TrAC Trends Anal. Chem.* **2020**, *127*, 115883.
[2] C. Yao, J. Qian, F. Chen, Y. Wang, J. Lin, J. Chen, J. Wei, Z. Yang, *Microchem. J.* **2023**, *193*, 109086.
[3] T. Mathai, T. Pal, N. Prakash, S. Mukherji, *Biosens. Bioelectron.* **2023**, *237*, 115478.
[4] M. Javed Ansari, D. Olegovich Bokov, S. Abdalkareem Jasim, M. Rudiansyah, W. Suksatan, G. Yasin, S. Chupradit, A. F. Alkaim, Y. F. Mustafa, D. Imad Tarek, *J. Mol. Liq.* **2022**, *354*, 118895.
[5] N. R. Moghadam, S. R. Arefhosseini, A. Javadi, F. Lotfipur, M. Ansarin, E. Tamizi, M. Nemati, *Iran. J. Pharm. Res.* **2018**, *17*, 1182–1190.
[6] R. Ghasemi, H. Mirzaei, M. R. Afshar Mogaddam, J. Khandaghi, A. Javadi, *Microchem. J.* **2022**, *181*, 107764.
[7] A. Kumar, A. K. Panda, N. Sharma, *J. Food Sci. Technol.* **2022**, *59*, 95–104.
[8] J. Zhou, Z. Xu, *Anal. Methods.* **2022**, 174–179.
[9] G. A. Saleh, H. F. Askal, I. H. Refaat, F. A. M. Abdelaal, *Asian J. Biomed. Pharm. Sci.* **2014**, *4*, 39–49.
[10] M. A. Mohammed, S. M. Abbas, J. M. S. Jamur, *Methods Objects Chem. Anal.* **2020**, *15*, 105–110.
[11] S. Bano, A. S. Ganie, R. I. A. Khan, S. Sultana, M. Z. Khan, S. Sabir, *Surfaces and Interfaces.* **2022**, *29*, 101786.
[12] R. Zokhtareh, M. Rahimnejad, G. Najafpour-Darzi, H. Karimi-Maleh, *Meas. J. Int. Meas. Confed.* **2023**, *215*, 112872.
[13] S. A. R. Alavi-tabari, M. A. Khalilzadeh, H. Karimi-maleh, *J. Electroanal. Chem.* **2018**, *811*, 84–88.
[14] S. M. Mostafavi, A. Rouhollahi, M. Adibi, A. Mohajeri, F. Pashaee, M. Pyriaee, *Asian J. Chem.* **2011**, *23*, 5247–5252.

[15] H. Teymourinia, A. Al-nayili, H. A. Alshamsi, R. Mohammadi, E. Sohouli, M. Gholami, *Surfaces and Interfaces.* **2023**, *42*, 103412.
[16] N. R. Jalal, T. Madrakian, A. Afkhami, M. Ghamsari, *J. Electroanal. Chem.* **2019**, *833*, 281–289.
[17] W. Sun, X. Wang, H. Zhu, X. Sun, F. Shi, G. Li, Z. Sun, *Sens. Actuators B* **2013**, *178*, 443–449.
[18] S. Taniselass, M. K. M. Arshad, S. C. B. Gopinath, *Biosens. Bioelectron.* **2019**, *130*, 276–292.
[19] H. Bagheri, H. Khoshsafar, S. Amidi, Y. Hosseinzadeh Ardakani, *Anal. Methods.* **2016**, *8*, 3383–3390.
[20] R. Chauhan, A. A. S. Gill, Z. Nate, R. Karpoormath, *J. Electroanal. Chem.* **2020**, *871*, 114254.
[21] E. Asadian, S. Shahrokhian, A. Iraji Zad, F. Ghorbani-Bidkorbeh, *Sens. Actuators B* **2017**, *239*, 617–627.
[22] W. Auwärter, *Surf. Sci. Rep.* **2019**, *74*, 1–95.
[23] N. L. McDougall, J. G. Partridge, R. J. Nicholls, S. P. Russo, D. G. McCulloch, *Phys. Rev. B.* **2017**, *96*, 1–9.
[24] D. Yan, Y. Li, J. Huo, R. Chen, L. Dai, S. Wang, *Adv. Mater.* **2017**, *29*, 1606459.
[25] Y. Mussa, F. Ahmed, M. Arsalan, E. Alsharaeh, *Sci. Rep.* **2020**, *10*, 1–13.
[26] H. Medetalibeyoğlu, M. Beytur, S. Manap, C. Karaman, F. Kardaş, O. Akyıldırım, G. Kotan, H. Yüksek, N. Atar, M. L. Yola, *ECS J. Solid State Sci. Technol.* **2020**, *9*, 101006.
[27] N. Atar, M. L. Yola, *J. Electrochem. Soc.* **2018**, *165*, H255–H262.
[28] T. Kokulnathan, T. J. Wang, M. Thangapandian, S. O. Alaswad, *Appl. Clay Sci.* **2020**, *187*, 105483.
[29] G. Kesavan, P. K. Gopi, S. M. Chen, V. Vinothkumar, *J. Electroanal. Chem.* **2021**, *882*, 114982.
[30] M. L. Yola, N. Atar, *Mater. Sci. Eng. C.* **2019**, *96*, 669–676.
[31] L. Zhou, L. Yang, C. Wang, H. Jia, J. Xue, Q. Wei, H. Ju, *Talanta.* **2022**, *238*, 123047.
[32] W. Da Oh, M. G. H. Lee, W. D. Chanaka Udayanga, A. Veksha, Y. Bao, A. Giannis, J. W. Lim, G. Lisak, *J. Environ. Chem. Eng.* **2019**, *7*, 102872.
[33] S. S. Laxmeshwar, S. S. Kulkarni, S. Nadaf, K. M. Swathi, H. M. Savanur, B. Chethan, V. Prasad, V. Jagadeesha Angadi, M. Ubaidullah, B. Pandit, L. Kansal, *J. Mater. Sci. Mater. Electron.* **2023**, *34*, 1–13.
[34] W. Oh, Z. Wong, X. Chen, K. A. Lin, A. Veksha, *Chem. Eng. J.* **2020**, *393*, 124714.
[35] X. Qiu, X. Wu, Y. Wu, Q. Liu, C. Huang, *RSC Adv.* **2016**, *6*, 106211–106217.
[36] B. Karupppaiah, A. Jeyaraman, S. M. Chen, Y. C. Huang, *Electrochim. Acta.* **2023**, *446*, 142008.
[37] C. Bhuvaneswari, K. Palpandi, B. Amritha, P. Paunkumar, R. Lakshmi Priya, N. Raman, S. Ganesh Babu, *Microchem. J.* **2023**, *184*, 108174.
[38] Y. Xie, Y. Peng, Y. Wang, D. Ma, Y. Cheng, L. Zhu, J. Han, X. Zhang, *J. Adv. Ceram.* **2023**, *12*, 24–35.
[39] K. Zhou, C. Chen, Y. Liu, S. Pang, N. Hua, W. Yang, T. Zhang, *Intermetallics.* **2017**, *90*, 81–89.
[40] Z. Jia, H. Li, Y. Zhao, D. A. Dikin, J. Ni, L. Zhao, J. Zhen, B. Ge, X. Shao, F. Ren, *J. Mater. Sci.* **2018**, *53*, 6562–6573.
[41] C. Zang, M. Yang, E. Liu, Q. Qian, J. Zhao, J. Zhen, R. Zhang, Z. Jia, W. Han, *Tribol. Int.* **2022**, *165*, 107312.
[42] M. Keerthana, T. Pushpa Malini, R. Sangavi, J. P. Arockia Selvi, M. Arthanareeswari, *ChemistrySelect.* **2022**, *7*, 1–12.
[43] N. Gissawong, S. Srijaranai, S. Boonchiangma, P. Uppachai, K. Seehamart, S. Jantrasee, E. Moore, S. Mukdasai, *Microchim. Acta.* **2021**, *188*, 208.
[44] F. L. Chen, K. H. Song, J. T. Xu, K. Z. Wang, X. Z. Feng, G. C. Han, H. B. Kraatz, *Sens. Actuators B* **2024**, *401*, 135008.
[45] M. V. Varsha, G. Nageswaran, *Microchem. J.* **2023**, *188*, 108481.
[46] A. G. Al-Harazie, E. A. Gomaa, R. R. Zaky, M. N. Abd El-Hady, *ACS Omega.* **2023**, *8*, 13605–13625.
[47] M. Wałęsa-Chorab, R. Banasz, D. Marcinkowski, M. Kubicki, V. Patroniak, *RSC Adv.* **2017**, *7*, 50858–50867.
[48] J. Wu, *Chem. Rev.* **2022**, *122*, 10821–10859.
[49] A. Tootoonchi, S. S. H. Davarani, R. Sedghi, A. Shaabani, H. R. Moazami, *J. Electrochem. Soc.* **2018**, *165*, B150–B159.
[50] A. Chaabani, T. Ben Jabrallah, N. Belhadj Tahar, *Electrocatalysis.* **2022**, *13*, 402–413.
[51] G. S. Garbellini, R. C. Rocha-Filho, O. Fatibello-Filho, *Anal. Methods.* **2015**, *7*, 3411–3418.
[52] S. A. Maier, *Springer* **2004**, *1*, 245.
[53] M. V. Smoluchowski, *Zeitschrift für Phys. Chemie.* **1918**, *92U*, 129–168.
[54] E. Laviron, *J. Electroanal. Chem.* **1974**, *52*, 395–402.
[55] R. Rani, A. Deep, B. Mizaikoff, S. Singh, *Electroanalysis.* **2020**, *32*, 2442–2451.
[56] X. Xing, J. Feng, G. Lv, K. Song, L. Mei, L. Liao, X. Wang, B. Xu, *Adv. Mater. Sci. Eng.* **2015**, *2015*, 148423.
[57] S. Zhang, S. Yu, X. Wang, Y. Zhang, Z. Yue, C. Li, Y. Ma, *Microchem. J.* **2023**, *194*, 109355.
[58] K. R. Reddy, P. K. Brahman, L. Suresh, *Meas. J. Int. Meas. Confed.* **2018**, *127*, 175–186.
[59] S. Tajik, H. Beitollahi, R. Zaeimbashi, M. Sheikhshoaei, M. B. Askari, P. Salarizadeh, *J. Mater. Sci. Mater. Electron.* **2021**, *32*, 17558–17567.
[60] J. V. Kumar, R. Karthik, S. M. Chen, V. Muthuraj, C. Karuppiah, *Sci. Rep.* **2016**, *6*, 34149.
[61] Reyhane Rahimpour, B. Sabeti, F. Chekin, *Russ. J. Electrochem.* **2021**, *57*, 654–662.
[62] W. D. Adane, B. S. Chandravanshi, M. Tessema, *Sens. Bio-Sensing Res.* **2023**, *39*, 100547.
[63] M. Pan, P. Guo, H. Liu, J. Lu, Q. Xie, *J. Anal. Sci. Technol.* **2021**, *12*, 55.
[64] K. Mariappan, S. Alagarsamy, S. M. Chen, S. Sakthinathan, *Materials.* **2023**, *16*, 741.

Manuscript received: February 26, 2024
Revised manuscript received: April 13, 2024
Version of record online: June 21, 2024